GSA DATA REPOSITORY 2012269

Negative C-isotope excursions at the Permian-Triassic boundary linked to volcanism

Jun Shen[1], Thomas J Algeo[2,*], Qing Hu[1], Ning Zhang[3], Lian Zhou[1], Wenchen Xia[3], Shucheng Xie[1], Qinglai Feng[1,*]

[1] State Key Laboratory of Geological Process and Mineral Resources, China University of Geosciences, Wuhan, Hubei, 430074, P.R. China

[2] Department of Geology, University of Cincinnati, Cincinnati, Ohio 45221-0013, U.S.A.

[3] Faculty of Earth Science, China University of Geosciences, Wuhan, Hubei, 430074, China

Methods

Samples collected in the field were trimmed to remove visible veins and weathered surfaces and pulverized to ~200 mesh size in an agate mortar. Major element abundances were determined by wavelength-dispersive X-ray fluorescence (XRF) analysis on fused glass beads using a XRF-1800 at the State Key Laboratory of Biogeology and Environmental Geology, China University of Geosciences (Wuhan). Trace elements and REEs were measured by Agilent 7500a inductively coupled plasma mass spectrometry (ICP-MS) at the State Key Laboratory of Geological Processes and Mineral Resources, China University of Geosciences (Wuhan). About 50 mg of each sample powder were weighed into a Teflon bomb and then moistened with a few drops of ultra-pure water before addition of 1 ml HNO_3 and 1 ml HF. The sealed bomb was heated at 190ºC in an oven for 48 hours. After cooling, the bomb was opened and evaporated at 115ºC to incipient dryness, then 1 ml HNO_3 was added and the sample was dried again. The resultant salt was re-dissolved with 3 ml 30% HNO_3 before it was again sealed and heated in the bomb at 190ºC for 12 hours. The final solution was transferred to a polyethylene bottle and diluted in 2% HNO_3 to about 80 ml for ICP-MS analysis. Analysis of the international rock standards BHVO-2 and BCR-2 indicated that the analytical precision is mostly better than 5%, according to the RSD.

Elemental C and S concentrations were measured on an Eltra 2000 C-S analyzer at the University of Cincinnati. An aliquot of each sample was digested in 2N HCl at 50°C for 12 hours to dissolve carbonate minerals, and the residue was analyzed for total organic carbon (TOC). Data quality was monitored via multiple analyses of the USGS SDO-1 standard, yielding an analytical precision (2σ) of ±2.5% of reported values for carbon.

Both organic and carbonate carbon isotopes were analyzed at the State Key Laboratory of Geological Processes and Mineral Resources, China University of Geosciences (Wuhan). Carbonate carbon isotopic compositions were determined according to the procedure of McCrea (1950). Samples were reacted offline with

100% H_3PO_4 for 24 hours at 250°C, following which the carbon isotope composition of the generated CO_2 was measured on a Finnigan MAT 251 mass spectrometer. All isotope data are reported as per mille (‰) relative to Vienna Pee Dee belemnite (V-PDB) standard. The analytical precision is better than ±0.1‰ for ^{13}C base on duplicate analyses. Organic carbon was separated by treating samples repeatedly with hot, concentrated HCl and HF to dissolve carbonates and silicates, and the acid-insoluble residue was separated using heavy liquids and washed to neutrality before recovering the organic carbon for isotopic analysis.

Biostratigraphic correlation of study sections with Meishan GSSP

The conodont biostratigraphy of the Xiakou section has been studied in detail by Wang and Xia (2004; W. Xia). Four biozones have been recognized: (1) *Clarkina changxingensis changxingensis-C. deflecta* Zone (originally Beds 223-256, here revised to Beds 223-251); (2) *Hindeodus latidentatus-C. meishanensis* Zone, comprising Beds (originally Beds 257-266, here revised to Beds 252-262); (3) *H. parvus* Zone (originally Beds 267-270, here revised to Beds 263-270); and (4) *Isarcicella isarcica* Zone (Beds 271-280) (Fig. 2). Samples from the *H. latidentatus-C. meishanensis* Zone yielded a particularly diverse conodont assemblage, including *C. deflecta*, *C. postwangi*, *C. wangi*, *C. subcarinata, C. changxingensis changxingensis*, and *C. changxingensis yini* in addition to the zone's eponymous species, constraining the position of the latest Permian mass extinction (LPME) horizon to below Bed 257 (Wang and Xia, 2004; Fig 2S). We have refined the position of the LPME based on C-isotope correlations, putting it at the Bed 251/252 contact (see below). The position of the Permian-Triassic boundary (PTB) was fixed based on the appearance of *H. parvus* at the base of Bed 267 (Wang and Xia, 2004), but more recent conodont studies (Xia unpubl. data) and C-isotope correlations (see below) have refined its position to the Bed 262/263 contact (Fig. 2).

At Xinmin, a preliminary reconnaissance of the conodont biostratigraphy has identified three zones (W. Xia, unpubl. data): (1) *C. changxingensis-C. postwangi* Zone, comprising Beds 1 and 2; (2) *C. yini* Zone, comprising Beds 3 and 4 and the lower part of Bed 5; and (3) *C. meishanensis* Zone, comprising the upper part of Bed 5 and the lower part of Bed 6 (Fig. 3). The index fossil *H. parvus* has not been recovered, but other fossil finds allow approximate placement of the PTB at Xinmin. The lower part of Bed 6 yielded the conodont *C. meishanensis*, the ammonoid *Huananoceras* sp., and the bivalve *Claraia primitive* Yin (Q.L. Feng, unpubl. data), an assemblage that confirms the latest Changhsingian (i.e., post-LPME) age of this unit. Recovery of a specimen of the ammonoid *Ophiceras* sp. from mid-Bed 6 suggests that the PTB is also located within this unit (Fig. 3).

The two study sections can be correlated to the GSSP at Meishan D on the basis of conodont biostratigraphy (Fig. S1). At Meishan, Bed 22 and the base of Bed 23 represent the upper part of the *C. changxingensis* Zone, mid-Bed 23 through Bed 24e the *C. yini* Zone, Beds 25-27b the *C. meishanensis* Zone, Beds 27c-d the *H. parvus*

Zone, Beds 28-29 the *I. staeschi* Zone, and Beds 30-51 the *I. isarcica* Zone (Zhang et al., 2007). The *C. changxingensis changxingensis*-*C. deflecta* Zone at Xiakou is the equivalent of the *C. changxingensis* and *C. yini* Zones at Meishan, confirming that the lower 2.7 m of the former section (Beds 223-251) is of late Changhsingian (but pre-LPME) age. The upper 1.9 m of this section (Beds 252-280) correlates with the *C. meishanensis*, *H. parvus*, and lower *I. isarcica* Zones at Meishan. The *C. changxingensis*-*C. postwangi* Zone at Xinmin is equivalent to the *C. changxingensis* Zone at Meishan, confirming that the lower ~7.7 m of the former section is of late Changhsingian (but pre-LPME) age. The *C. meishanensis* Zone represents the interval between the LPME and the PTB at Meishan, indicating a latest Changhsingian age for the lowermost Luolou Formation at Xinmin (Fig. 3). See Kozur (2004, 2005) and Algeo et al. (2012a,b) for reference conodont biozonation schemes.

C-isotopic correlation of study sections with Meishan GSSP

Within the framework established through conodont biostratigraphy (see above), carbon isotope profiles allow further refinement of correlations between the study sections and the Meishan GSSP. Cao et al. (2002) published reference curves for both $\delta^{13}C_{carb}$ and $\delta^{13}C_{org}$ at Meishan, and the $\delta^{13}C_{carb}$ profile was subsequently improved upon by Xie et al. (2007), allowing a direct comparison between the carbonate and organic C-isotope records for a single section with no uncertainty regarding relative stratigraphic placement of samples. The profiles show markedly different patterns of C-isotopic variation (Fig. S1). First, the $\delta^{13}C_{org}$ profile exhibits an earlier and more rapid shift toward lower values within the *C. yini* Zone than the $\delta^{13}C_{carb}$ profile. Second, following abrupt excursions to minima in both profiles immediately above the LPME, the $\delta^{13}C_{org}$ curve shifts toward more ^{13}C-enriched (and more variable) values in the lowermost Triassic, whereas the $\delta^{13}C_{carb}$ profile exhibits a trend toward more ^{13}C-depleted values (with minimal variability) in the same interval. Owing to these differences, it is essential that a single type of C-isotope record ($\delta^{13}C_{carb}$ or $\delta^{13}C_{org}$) be used for correlations between sections.

The carbonate C-isotope record for Xiakou exhibits an overlapping range of values (ca. -1 to +3‰) and similar features to the Meishan reference curve (Fig. S1). Both sections exhibit a shift toward higher $\delta^{13}C_{carb}$ values in the upper *C. changxingensis* Zone, although this shift is more pronounced at Xiakou and ash layers correlative to VI-1 to VI-3 have not been reported from Meishan. Both profiles exhibit a slow shift toward more ^{13}C-depleted values within the *C. yini* Zone, although the shift commences somewhat earlier at Meishan than at Xiakou. This gradual negative trend continues to just below the LPME, a pattern that is characteristic of many PTB sections globally (Korte and Kozur, 2010; Luo et al., 2011). A local minimum (corresponding to VI-4 at Xiakou and upper Bed 24d at Meishan) is found toward the top of the *C. yini* Zone and may be correlative between the sections. Both records exhibit a rapid negative excursion at the LPME, followed by a recovery to more positive values within the *C. meishanensis* Zone. Above the PTB, the two $\delta^{13}C_{carb}$

profiles are less similar, although the sections may be correlatable on the basis of ash-bed stratigraphy: both sections exhibit a pair of ash layers (VI-8 and VI-9 at Xiakou, Beds 31 and 33 at Meishan) in the lowermost *I. isarcica* Zone.

The organic C-isotope record for Xinmin shows some similarities to the Meishan reference curve, although $\delta^{13}C_{org}$ values are generally 3-6‰ heavier in the correlative intervals at Xinmin (Fig. S1). Both profiles exhibit a weak shift toward more ^{13}C-enriched values in the upper *C. changxingensis* Zone (n.b., correlative with a similar shift in $\delta^{13}C_{carb}$ profiles). A strong shift toward more negative $\delta^{13}C_{org}$ values in the lower *C. yini* Zone at Meishan is not seen at Xinmin, although this zone is characterized by frequent sharp $\delta^{13}C_{org}$ minima associated with ash layers; it is unclear how these two different C-isotopic patterns are related. Both profiles exhibit a strong negative excursion at the LPME followed by a recovery to more positive values within the *C. meishanensis* Zone. Above the PTB, the relationship between the two curves is unclear: both show increased sample-to-sample variance, although the *H. parvus-I. staeschi* Zones are marked by a sustained shift toward heavier values at Meishan and lighter values at Xinmin. The trend toward heavier values at Meishan is an anomaly; the correlative interval of most PTB sections is characterized by lighter $\delta^{13}C_{org}$ values, as at Shangsi, China (Riccardi et al., 2007), Heping and Taiping, China (Krull et al., 2004), Slovenia (Schwab and Spangenberg, 2004), and Sverdrup Basin sections in the Canadian Arctic (Grasby and Beauchamp, 2008; Algeo et al., 2012a). Also unclear is whether the VA-12 to VA-14 ash layers at Xinmin should be correlated with Meishan's Bed 28 (as shown) or with Beds 31 and 33 (implying condensation of post-PTB strata at Xinmin).

Paleoproductivity proxies versus C-isotopic composition

We investigated possible marine productivity controls on organic matter accumulation in the study sections by examining covariation between $\delta^{13}C$ ($\delta^{13}C_{carb}$ for Xiakou, $\delta^{13}C_{org}$ for Xinmin) versus paleoproductivity proxies (TOC, P, and Ba_{xs}; Fig. S2). Neither section exhibits a statistically significant correlation between $\delta^{13}C$ and TOC or P, and Xinmin does not exhibit a correlation between $\delta^{13}C$ and Ba_{xs}. The only significant relationship is a modest one between $\delta^{13}C_{carb}$ and Ba_{xs} at Xiakou (r^2 = 0.23). Although not conclusive, the general absence of relationships between $\delta^{13}C$ and paleoproductivity proxies in the two study sections is consistent with the inference that C-isotopic variation was not strongly influenced by variations in marine primary productivity.

Both sections exhibit relatively low levels of thermal maturity based on a range of proxies. The Xiakou section yielded vitrinite reflectances (R_o) of <1.0% and conodont color alteration indices (CAI) of <2.0, equivalent to maximum burial temperatures of 50-90°C (Du, 1983). The Xinmin section yielded R_o of ~2% and CAI of 2.0-2.5, equivalent to maximum burial temperatures of ~100°C (Zhou, 1985). Total organic carbon (TOC) values are substantial, especially at Xiakou (average TOC = 1.37%). These relatively low levels of thermal maturity are consistent with minimal loss of organic carbon during burial.

References

Algeo, T., Henderson, C.M., Ellwood, B., Rowe, H., Elswick, E., Bates, S., Lyons, T., Hower, J.C., Smith, C., Maynard, B., Hays, L.E., Summons, R.E., Fulton, J., and Freeman, K.H., 2012a, Evidence for a diachronous Late Permian marine crisis from the Canadian Arctic region: Geological Society of America Bulletin, publ. online 6 February 2012, doi:10.1130/B30505.1.

Algeo, T.J., Henderson, C.M., Tong, J.N, Feng, Q.L, Yin, H.F, and Tyson, R.V., 2012b, Plankton and productivity during the Permian-Triassic boundary crisis: An analysis of organic carbon fluxes: Global and Planetary Change, in press.

Cao, C., Wang, W., and Jin, Y., 2002, Carbon isotope excursions across the Permian-Triassic boundary in the Meishan section, Zhejiang Province, China: Chinese Science Bulletin, v. 47, p. 1125-1129.

Du, G., 1983, On the color alteration of conodonts and maturity of organic matter in the Permian and Triassic systems of Hubei Province: Acta Petrolei Sinica, v. 4, p. 11-18 (in Chinese).

Grasby, S.E., and Beauchamp, B., 2008, Intrabasin variability of the carbon-isotope record across the Permian-Triassic transition, Sverdrup Basin, Arctic Canada: Chemical Geology, v. 253, p. 141-150.

Korte, C., and Kozur, H.W., 2010, Carbon-isotope stratigraphy across the Permian-Triassic boundary: a review: Journal of Asian Earth Science, v. 39, p. 215-235.

Kozur, H.W., 2004, Pelagic uppermost Permian and Permian-Triassic boundary conodonts of Iran. Part I. Taxonomy: Hallesches Jahrbuch für Geowissenschaften, Reihe B: Geologie, Palaontologie, Mineralogie, v. 18, p. 29-68.

Kozur, H.W., 2005, Pelagic uppermost Permian and Permian-Triassic boundary conodonts of Iran. Part II. Investigated sections and evaluation of the conodont faunas: Hallesches Jahrbuch für Geowissenschaften, Reihe B: Geologie, Palaontologie, Mineralogie, v. 19, p. 49-86.

Krull, E.S., Lehrmann, D.J., Druke, D., Kessel, B., Yu, Y., and Li, R., 2004, Stable carbon isotope stratigraphy across the Permian-Triassic boundary in shallow marine carbonate platforms, Nanpanjiang Basin, south China: Palaeogeography Palaeoclimatology Palaeoecology, v. 204, p. 297-315.

Luo, G., Wang, Y., Yang, H., Algeo, T.J., Kump, L.R., Huang, J., and Xie, S., 2011, Stepwise and large-magnitude negative shift in $\delta^{13}C_{carb}$ preceded the main marine mass extinction of the Permian-Triassic crisis interval: Palaeogeography Palaeoclimatology Palaeoecology, v. 299, p. 70-82.

McCrea, J.M., 1950, On the isotope chemistry of carbonates and a paleotemperature scale: The Journal of Chemical Physics, v.18, p. 849-857.

Riccardi, A., Kump, L.R., Arthur, M.A., and D'Hondt, S., 2007, Carbon isotopic evidence for chemocline upward excursions during the end-Permian event: Palaeogeography, Palaeoclimatology, Palaeoecology, v. 248, p. 73-81.

Schwab, V., and Spangenberg, J.E., 2004, Organic geochemistry across the Permian-Triassic transition at the Idrijca Valley, western Slovenia: Applied Geochemistry, v. 19, p. 55-72.

Shen, J., Algeo, T., Hu, Q., Xu, G., Zhou, L., and Feng, Q., 2012b, Volcanism in South China during the Late Permian and its relationship to marine ecosystem and environmental changes: Global and Planetary Change, in press.

Shen, J., Algeo, T.J., Zhou, L., Feng, Q., Yu, J., and Ellwood, B.B., 2012a, Volcanic perturbations of the marine environment in South China preceding the latest Permian extinction event and their biotic effects: Geobiology, v. 10, p. 82-103.

Shen, S.-, Crowley, J.L., Wang, Y., Bowring, S.A., Erwin, D.H., Sadler, P.M., Cao, C., Rothman, D.H., Henderson, C.M., Ramezani, J., Zhang, H., Shen, Y., Wang, X., Wang, W., Mu, L., Li, W., Tang, Y., Liu, X., Liu, L., Zeng, Y., Jiang, Y., and Jin, Y., 2011, Calibrating the end-Permian mass extinction: Science, v. 334, p. 1367-1372.

Wang, G., and Xia, W., 2004, Conodont zonation across the Permian-Triassic boundary at the Xiakou section, Yichang city, Hubei Province, and its correlation with the global stratotype section and point of the PTB: Canadian Journal of Earth Science, v. 41, p. 323-330.

Xie, S., Pancost, R.D., Huang, J., Wignall, P.B., Yu, J., Tang, X., Chen, L., Huang, X., and Lai, X., 2007, Changes in the global carbon cycle occurred as two episodes during the Permian-Triassic crisis: Geology, v. 35, p. 1083-1086.

Zhang, K., Tong, J., Shi, G.R., Lai, X., Yu, J., He, W., Peng, Y., and Jin, Y., 2007, Early Triassic conodont-palynological biostratigraphy of the Meishan D section in Changhsing, Zhejiang Province, South China: Palaeogeography, Palaeoclimatology, Palaeoecology, v. 252, p. 4-23.

Zhou, X., 1985, Permian and Triassic conodont color alteration and its petroleum geological significance in Guizhou Province: Journal of Southwestern Petroleum Institute, v. 22, p. 1-13 (in Chinese).

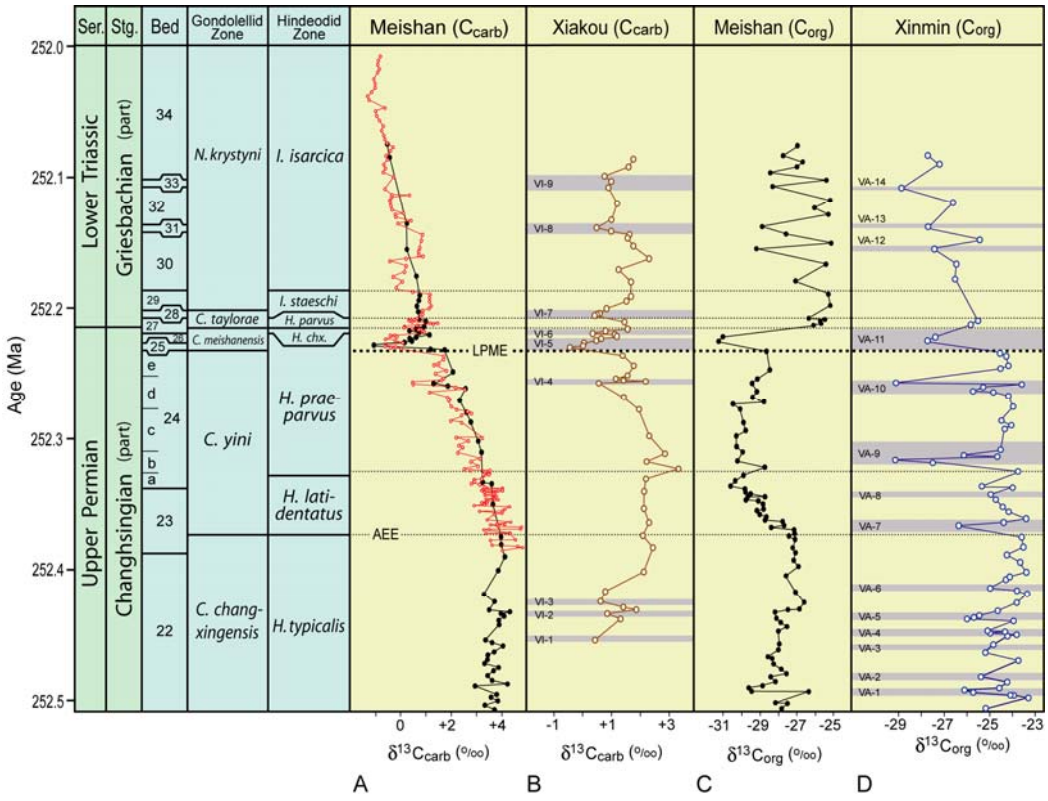

Figure DR1. Comparison of C-isotopic profiles for (A) $\delta^{13}C_{carb}$ at Meishan D, (B) $\delta^{13}C_{carb}$ at Xiakou, (C) $\delta^{13}C_{org}$ at Meishan D, and (D) $\delta^{13}C_{org}$ at Xinmin. Sources: A is from Cao et al. (2002; black symbols) and Xie et al. (2007; red symbols), B is original to this study, C is from Cao et al. (2002), and D is from Shen et al. (2012b). The C-isotope profiles for Meishan were rescaled to the PTB timescale of Algeo et al. (2012a,b), which has key tie-points at 252.28±0.8 Ma and 252.17±0.6 Ma for the LPME and PTB, respectively (based on Shen et al., 2011). The Xiakou and Xinmin profiles were then correlated to the Meishan profiles based on existing biostratigraphic constraints (discussed in text). Abbreviations: AEE = Arctic extinction event (Algeo et al., 2012a); LPME = latest Permian mass extinction; PTB = Permian-Triassic boundary; VA = volcanic ash layer (Xinmin); VI = volcanic interval (Xiakou); (conodont zones) *C.* = *Clarkina*, *H.* = *Hindeodus*, *I.* = *Isarcicella*, *chx.* = *changxingensis*, *lat.* = *latidentatus*, and *meish.* = *meishanensis*.

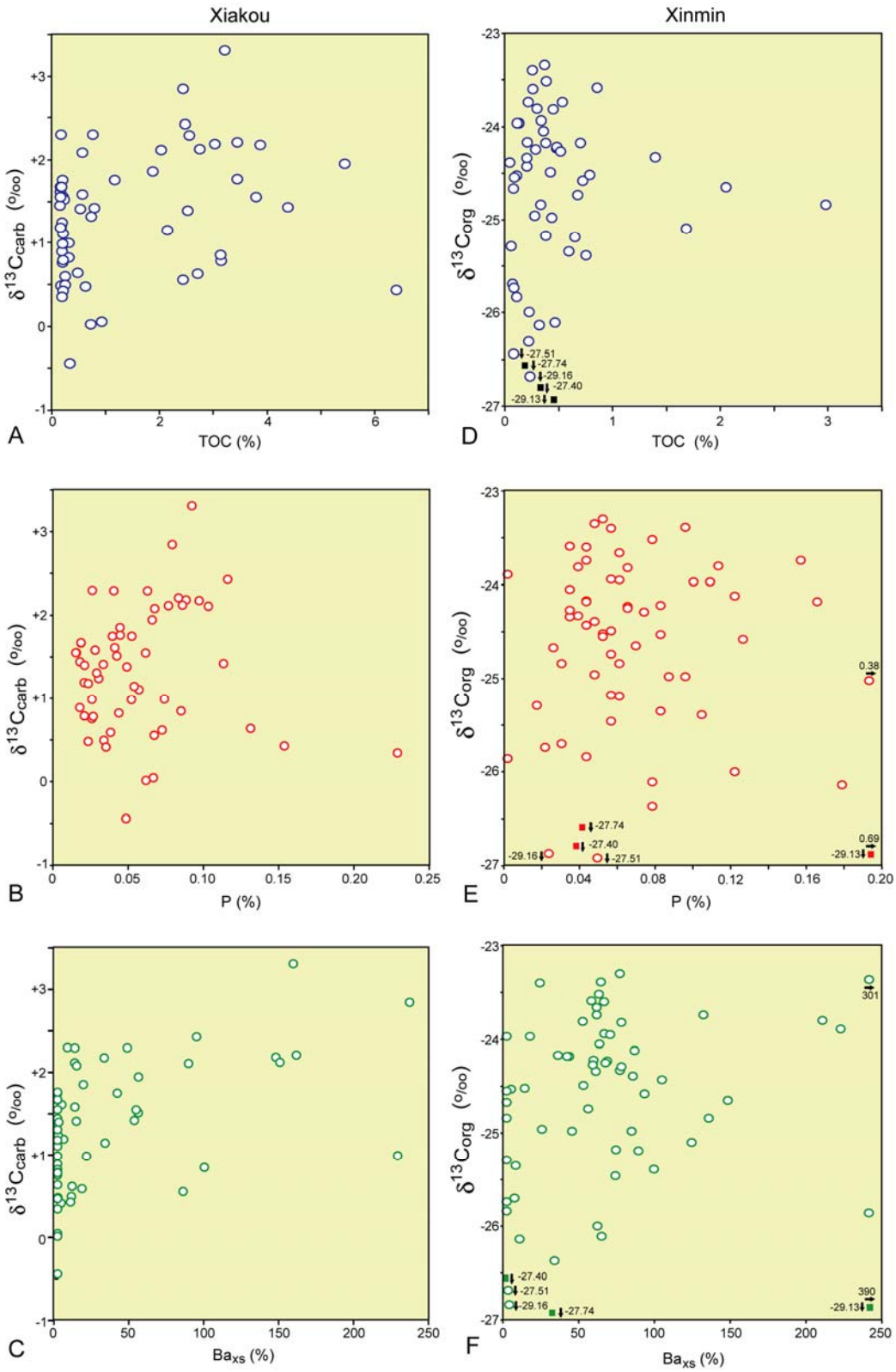

Figure DR2. $\delta^{13}C_{carb}$ versus (A) TOC, (B) P, and (C) Ba_{xs} for Xiakou, and $\delta^{13}C_{org}$ versus (D) TOC, (E) P, and (F) Ba_{xs} for Xinmin. TOC, P, and Ba_{xs} (excess Ba)

are paleoproductivity proxies; Ba_{xs} was calculated as $Ba_{meas} - Al_{meas} \times m$, where m represents the minimum slope on a Ba-Al crossplot (m = 30 for Xiakou and 16 for Xinmin; units of ppm/% or 10^{-4}; cf. Shen et al., 2012a). Note the lack of statistically significant covariation in all graphs except C, which yielded r^2 = 0.23 ($p(\alpha)$ <0.01; n = 67). These results suggest that marine productivity was not a strong influence on the C-isotopic compositions of the study sections.